Inertial particle separation by differential equilibrium positions in a symmetrical serpentine microchannel

Jun Zhang[1], Sheng Yan[1], Ronald Sluyter[2,3], Weihua Li[1]*, Gursel Alici[1] & Nam-Trung Nguyen[4]*

[1]School of Mechanical, Materials and Mechatronic Engineering, University of Wollongong, Wollongong, NSW 2522, Australia.

[2]School of Biological Sciences, University of Wollongong, Wollongong, NSW 2522, Australia

[3]Illawarra Health and Medical Research Institute, Wollongong, NSW 2522, Australia

[4]Queensland Micro and Nanotechnology Centre, Griffith University, Brisbane QLD 4111, Australia.

Supplementary informations

(1) Supplementary Fig. S1

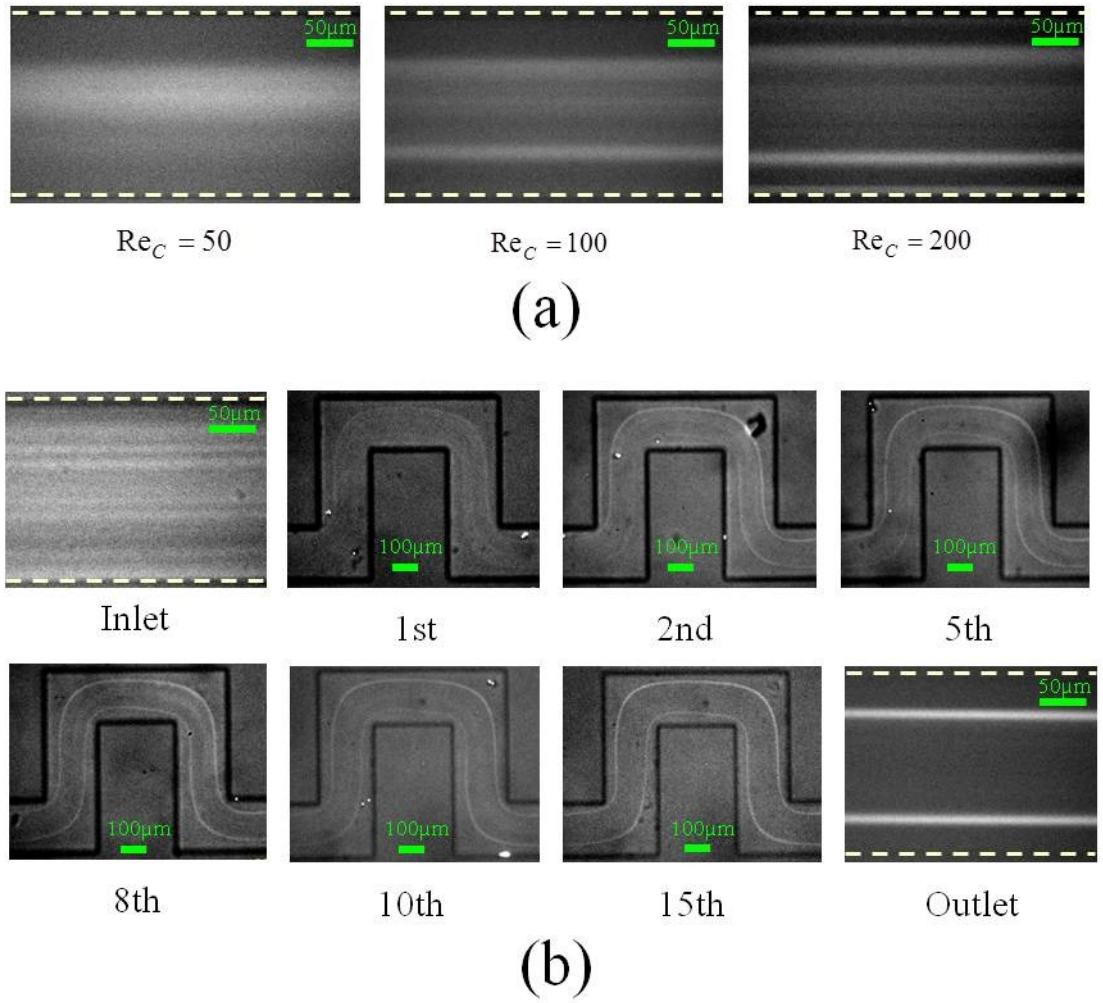

Fig. S1 (a) Fluorescent images of particles at a 40 mm distance from inlet in a straight channel. No distinct focusing positions can be observed when Re_C=50. And even at a much larger Reynolds number 100 and 200, inertial focusing is still not achieved completely within 40 mm length. (b) Fluorescent images of particles in different periods of a serpentine channel when Re_C=50. Particles are effectively focused at two sides after about 10th period, with a length about 10 mm. Particle diameter is 10 μm.

(2) Supplementary Fig. S2

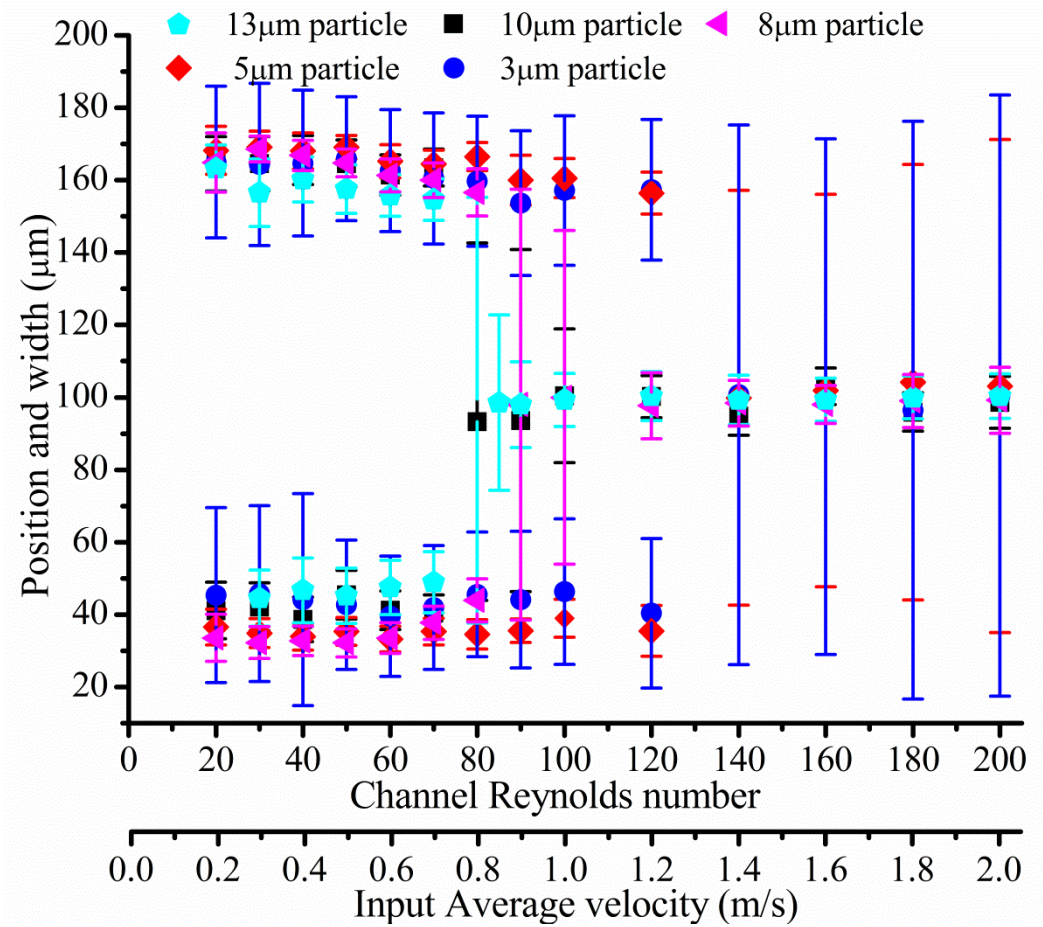

Fig. S2 Focusing positions and widths for different-sized particles under various flow conditions. Error bars indicate the streak width, which was determined by standard FWHM (full width at half maximum). The streak position was taken as the middle of the half maximum intensity.

(3) Supplementary Fig. S3

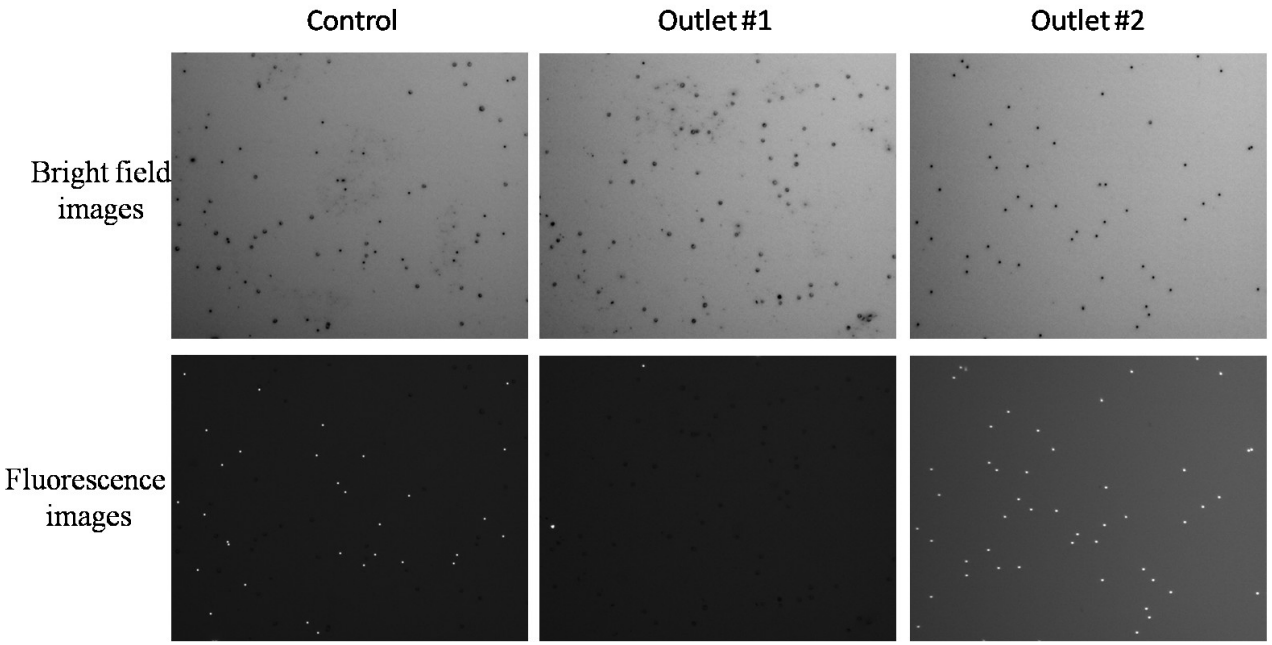

Fig. S3 The bright field and fluorescence images from control and two collections. In bright field image, both of MEL cells and 5-μm polystyrene beads can be observed. While in fluorescent images, only 5-μm fluorescent polystyrene beads can be observed. The number of MEL cells can be easily obtained by subtracting number of 5-μm polystyrene beads from the total number of MEL cells and 5-μm polystyrene beads.

(4) Supplementary Fig. S4

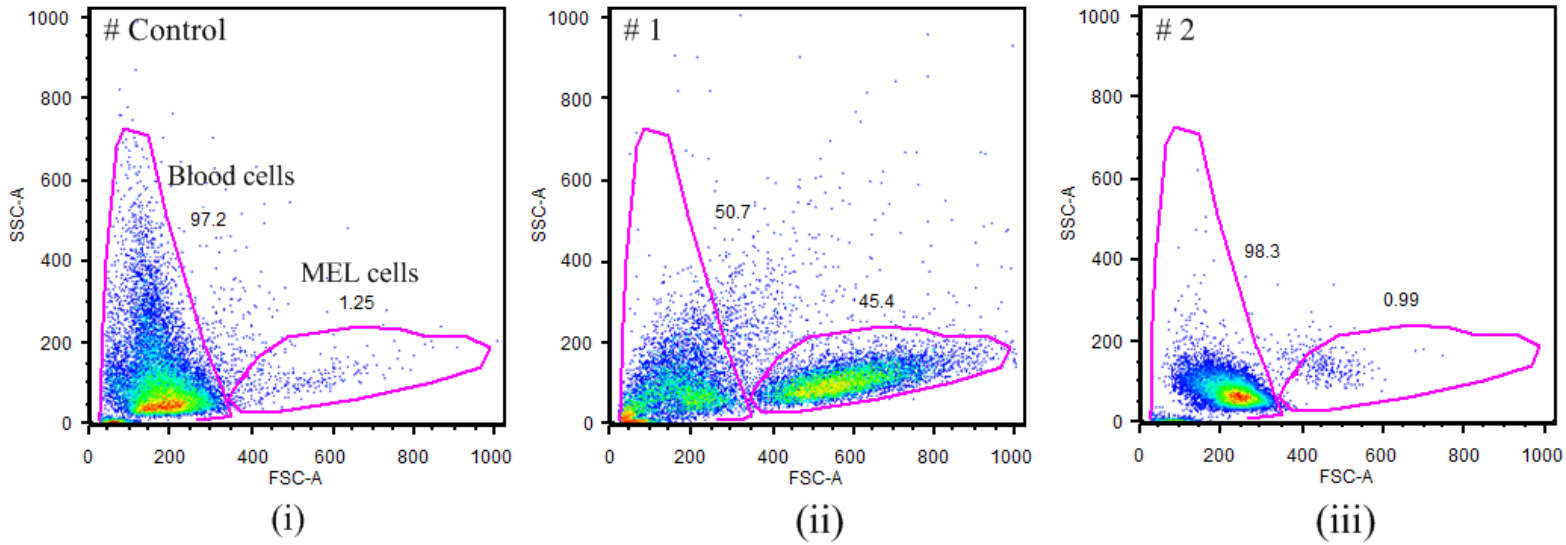

Fig. S4 Flow cytometric data show the results of separation of MEL cells and human blood cells in the serpentine channel. The MEL cell purity was increased from 1.25% to 45.4%, causing an impressive enrichment ratio (collection purity/input purity) of 36.32

(5) Supplementary Fig. S5

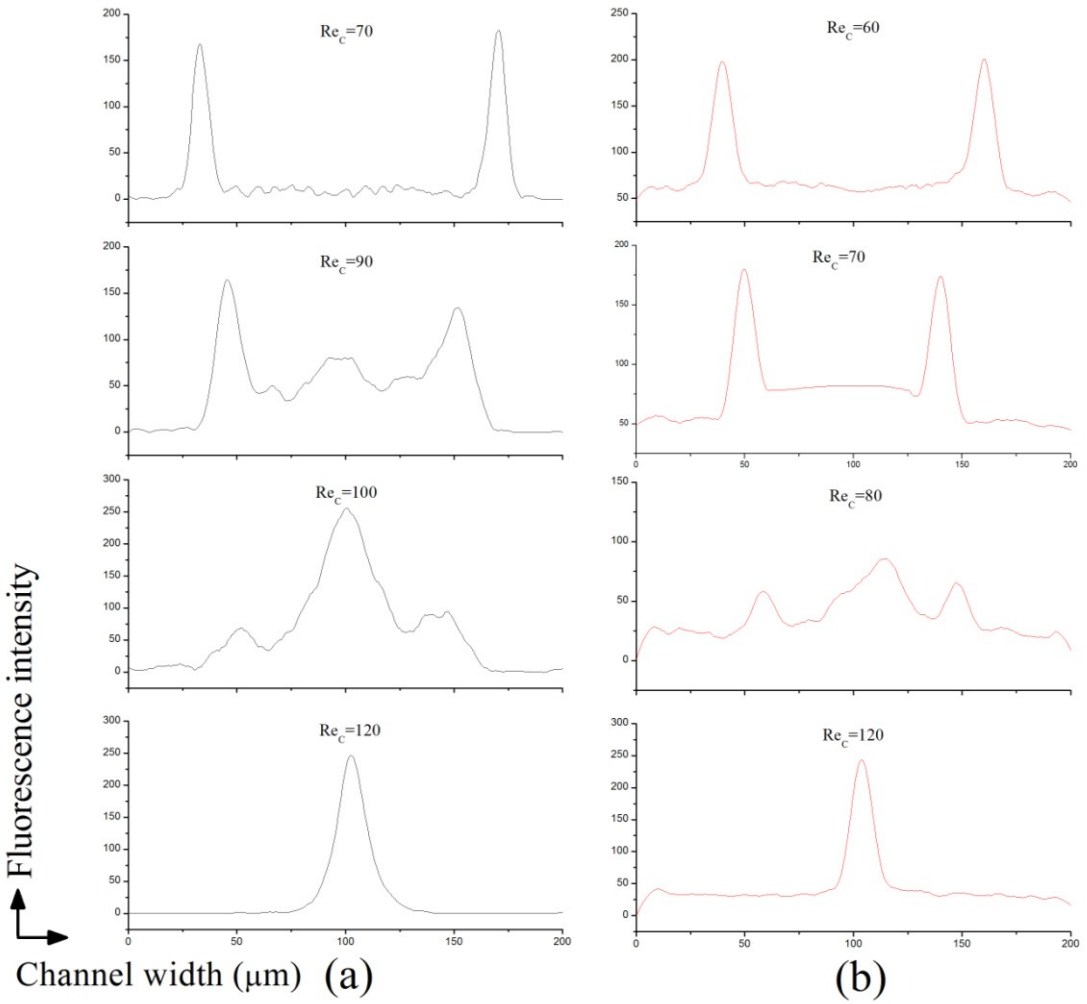

Fig. S5 The fluorescence profile within the transition region II for (a) 8-μm and (b) 10-μm polystyrene particles. At the beginning of this region, besides two sided focusing streaks, another weak focusing streak arises at the centre of channel, which is expected to be the initial result of DC force. Most of the particles are on these three regions, with few particles distributed within the gaps between them. Increasing the flow rate, the

two sided focusing streaks get closer to the channel centre with decreasing intensity, while the intensity of central focusing streak increases. Finally, three streaks merge together to a single central focusing streak.

(6) Supplementary Fig. S6

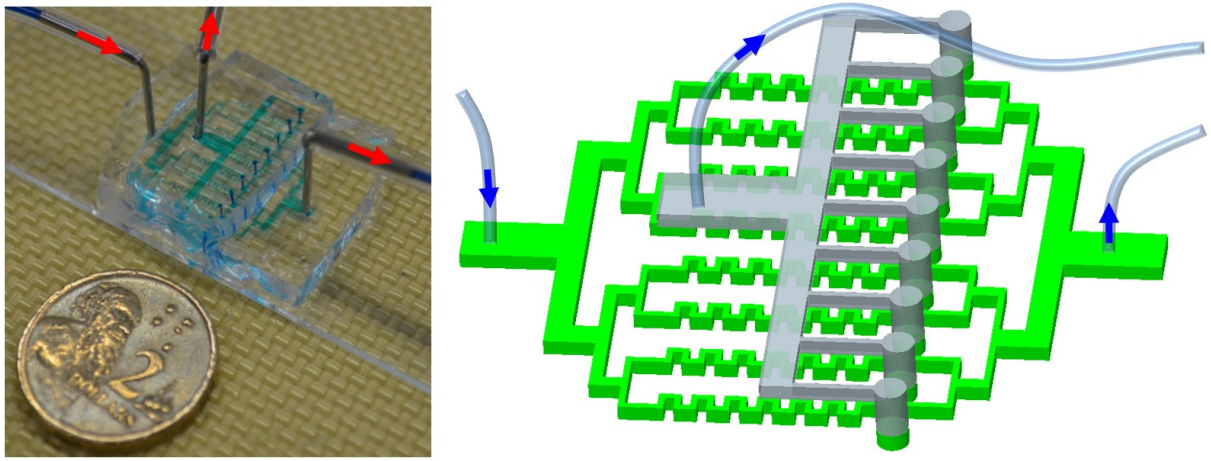

Fig. S6 A parallelized inertial microfluidic device with eight serpentine channels. (Left) fabricated device, and (right) schematic structure. The device was fabricated by two layers. The serpentine channels are in the bottom layers to separate particles by size, and larger particles are collected by central branch. The up layer is to collect smaller particles from two sided branches. In this device, the working throughput can be as high as 4.8 ml/min.

(7) Supplementary Text- analysis of three focusing patterns

Inertial migration is a phenomenon where randomly dispersed particles in the entrance of a straight channel migrate laterally to several cross-sectional equilibrium positions after a long enough distance [1-2]. Two dominant forces are responsible for this phenomenon: the shear gradient lift force F_{LS} acting down the velocity gradient towards the channel walls, and a wall induced lift force F_{LW} directed towards the centreline of the channel. The balance of these two forces creates several equilibrium positions in the cross section. The net inertial lift force can be expressed as [3-4]:

$$F_L = \frac{f_L \rho_f U_m^2 a^4}{D_h^2} \tag{1}$$

$$\mathrm{Re}_C = \frac{\rho_f U_m D_h}{\mu} \tag{2}$$

where ρ_f, U_m and μ are the fluid density, maximum velocity and dynamic viscosity, respectively. The spherical particles have a diameter a. The hydraulic diameter D_h of the channel is defined as D_h=2WH/(W+H) for a rectangular channel (W and H correspond to width and height of the rectangular cross-section). The lift coefficient f_L is a function of the particle position x_C, channel Reynolds number Re_C and particle size a [4-5]. In a square straight channel (AR=height/width=1), particles focus to four equilibrium positions, at the centre of each face. A further reduction to two equilibrium positions happens when aspect ratio (AR) ranges between 1/3 and 1/2 channel, due to the blunted velocity profile along the long face of the channel and corresponding reduction of shear gradient lift force [6].

When particles flow within a curved microchannel, they also experience an additional drag force exerted by a secondary flow (Dean vortex) within the cross section of channel. This secondary flow arises due to the channel curvilinear geometry and non-negligible inertia of fluid [7], and its magnitude can be evaluated by the non-dimensional Dean number (De). The Dean drag force tends to entrain particles following fluid streamlines, and can be quantified based on the Stokes law.

$$De = \frac{\rho_f U_f D_h}{\mu} \sqrt{\frac{D_h}{2R}} = \mathrm{Re} \sqrt{\frac{D_h}{2R}} \tag{3}$$

$$U_D = 1.8 \times 10^{-4} \times De^{1.63} \tag{4}$$

$$F_D = 3\pi\mu a (v_f - v_p) \tag{5}$$

where R is the radius of channel curvature and Re is the flow Reynolds number which is defined based on average fluid velocity U_f [8]. U_D is average velocity of Dean flow. v_f and v_p represent cross-sectional velocity of fluid and particles respectively.

Equation (5) can be further simplified when particles are focused and steady within channel cross-section.

$$F_D = 3\pi\mu a U_D = 5.4\times10^{-4}\pi\mu a De^{1.63} \tag{6}$$

Besides, particle centrifugal force in serpentine channel can play a significant effect on particle movement as we studied [9].

$$F_{Cent} = (\rho_p - \rho_f)\pi a^3 v_{pt}^2 / 6R \tag{7}$$

where ρ_p and v_{pt} are the density and tangential velocity of particles in curved channel, respectively.

The ratio ε of DC force (F_{Cent}+F_D) to inertial lift force (F_L) determines the focusing patterns of particles in a serpentine microchannel. With ε>>1, DC force will dominate the movement of particles, and particles are focused at the centre of channel. In contrast, with ε<<1, inertial lift force will decide the trajectory of particles, and particles are expected to focus at two sides of channel. The ratio ε can be expressed as:

$$\varepsilon = \frac{F_D + F_{Cent}}{F_L} \approx A(\rho_f, D_h, R, \mu)a^{-1}U_f^{0.13} + B(\rho_f, \rho_P, R, D_h)aU_f^{0.5} \tag{8}$$

As $f_L \propto \frac{1}{a^2\sqrt{\mathrm{Re}}}$ [5]

From equation (8), ε is proportional to U_f. So ε increases with increasing flow rate (or U_f), it agrees well with the experimental observation, where particle focusing pattern transferred from two sided focusing streaks to central band focusing and finally central single focusing streak when increasing flow rate continuously. However, equation (8) still cannot figure out the exact trend of ε with particle size a, it seems that ε is proportional to particle size from the experimental results.

Supplementary Table S1 Comparison of existing inertial microfluidic techniques for binary-particle separation

Channel Type	Throughput	Purity	Efficiency	Channel dimension	Device footprint	Particle size/cell type	Size difference (Resolution)	Need sheath flow?	Parallelizability	Reference
Straight	Re=40 (100μlmin-1)	20-μm particle 90.8% 9.94-μm 99.6%	20-μm particle 99.3% 9.94-μm 94.5%	27μm×50μm (width×height) upstream 100μm×50μm downstream	Straight micro-channel section >36mm	9.9-μm, 20-μm polystyrene beads	~10 μm	No	Good	10
	40 parallel channels with 240ml/h, 4×10^8 cells/min	NA	88% red blood cells (RBCs) E Coli: NA	20μm×60μm upstream 160μm×60μm down stream	7cm×7cm	RBCs~8 μm Eschericha coli ~1 μm	~7 μm	No	Good	11
Expansion-contraction array	111 beads/s	10-μm particle 100% 4-μm particle 99%	NA	CEA 350μm ×38μm (width ×height) Contraction region 50μm ×300μm (width×length)	Micro-channel length >9 mm	4-μm, 10-μm polystyrene beads	6 μm	Yes	Good	12
	$1.1x10^8$ cells/min Re=8	Blood cell reject ratio 88.9%	Cancer cells: 99.1% Blood cells: NA	CEA 350μm ×63μm (width ×height) Contraction region 50μm ×1200μm (width×length)	Micro-channel length >11.4 mm	MCF-7 , blood cells	NA	Yes	Good	13
Spiral	3 ml/hr	NA	Cancer cell lines >85% Blood cells: NA	Spiral channel 500μm×160μm	Total micro-channel length ~10cm	MCF-7, Hela, MDA-MB-231	NA	Yes	Hard	14
	7.5 ml blood within 8 mins	NA	>80% Blood cells:NA	Width 100 μm Inner/outer height 80μ/130μm	NA	T24, MVF-7, MDA-MB-231	NA	No	Hard	15
Double spiral	3.33×10^7 cells/min	NA	99.66%: 5μm particles 92.75%: 15μm particles 88.5% tumor recovery	300 μm in width and 50 μm in height The radius of the outermost curvature is 9 mm	NA	5-μm, 15-μm polystyrene beads MCF-7 and Hela cells spiked in whole blood	10 μm	No	Hard	16
Asymmetric serpentine	0.9 ml/min Rp=1.53	9-μm particle: 16.3% one tier, 25.3% Two tier processes 3.1-μm particle: ~99.9% after two tiers	3.1-μm: ~56% after two tiers; 9-μm:NA	Height: 50μm Width: 100~650μm	Channel length ~6.9cm	3.1 and 9-μm polystyrene beads	~6μm	No	Good	17
Proposed device with symmetric serpentine in this work	600 μl/min Re=120 4.8ml/min for 8 parallel serpentine channels	3-μm:~99% 10-μm:~88.7% 5-μm:~99.2% 13-μm:~~91.6% 5-μm:~98% MEL cells:~94.9%	Large particles:>97% Small particles:>92%	200μm×42μm (width×height)	Whole device: 36 mm×5mm (length ×width); Serpentine channel with a length of ~15mm, this value can further reduced to ≤10mm. Device with 8 parallel channel: 30mm×23mm	3,5, 10 and 13-μm polystyrene beads and MEL cells Human blood cells and MEL cells	~7μm demonstrated; ≤ 3μm in principle	No	Good	This paper

References:

1 Segre, G. Radial particle displacements in Poiseuille flow of suspensions. *Nature* **189**, 209-210 (1961).
2 Segre, G. & Silberberg, A. Behaviour of macroscopic rigid spheres in Poiseuille flow Part 2. Experimental results and interpretation. *J. Fluid Mech.* **14**, 136-157 (1962).
3 ASMOLOV, E. S. The inertial lift on a spherical particle in a plane Poiseuille flow at large channel Reynolds number. *J. Fluid Mech.* **381**, 63-87 (1999).
4 Di Carlo, D. Inertial microfluidics. *Lab Chip* **9**, 3038-3046 (2009).
5 Zhou, J. & Papautsky, I. Fundamentals of inertial focusing in microchannels. *Lab Chip* **13**, 1121-1132 (2013).
6 Chung, A. J., Gossett, D. R. & Di Carlo, D. Three Dimensional, Sheathless, and High-Throughput Microparticle Inertial Focusing Through Geometry-Induced Secondary Flows. *Small* **9**, 685-690 (2013).
7 Amini, H. *et al.* Engineering fluid flow using sequenced microstructures. *Nat. Commun.* **4**, 1826 (2013).
8 Bhagat, A. A. S., Kuntaegowdanahalli, S. S. & Papautsky, I. Continuous particle separation in spiral microchannels using dean flows and differential migration. *Lab Chip* **8**, 1906-1914 (2008).
9 Zhang, J., Li, W., Li, M., Alici, G. & Nguyen, N.-T. Particle inertial focusing and its mechanism in a serpentine microchannel. *Microfluid. Nanofluid.*, 1-12, doi: 10.1007/s10404-013-1306-6 (2013).
10 Zhou, J., Giridhar, P. V., Kasper, S. & Papautsky, I. Modulation of aspect ratio for complete separation in an inertial microfluidic channel. *Lab Chip* **13**, 1919-1929 (2013).
11 Mach, A. J. & Di Carlo, D. Continuous scalable blood filtration device using inertial microfluidics. *Biotechnol. Bioeng.* **107**, 302-311 (2010).
12 Lee, M. G., Choi, S. & Park, J. K. Inertial separation in a contraction–expansion array microchannel. *J. Chromatogr. A* **1218**, 4138-4143 (2011).
13 Lee, M. G., Shin, J. H., Bae, C. Y., Choi, S. & Park, J.-K. Label-Free Cancer Cell Separation from Human Whole Blood Using Inertial Microfluidics at Low Shear Stress. *Anal. Chem.* **85**, 6213-6218 (2013).
14 Hou, H. W. *et al.* Isolation and retrieval of circulating tumor cells using centrifugal forces. *Scientific reports* **3**, 1259 (2013).
15 Warkiani, M. E. *et al.* Slanted spiral microfluidics for the ultra-fast, label-free isolation of circulating tumor cells. *Lab Chip* **14**, 128-137 (2014).
16 Sun, J. *et al.* Double spiral microchannel for label-free tumor cell separation and enrichment. *Lab Chip* **12**, 3952-3960 (2012).
17 Di Carlo, D., Edd, J. F., Irimia, D., Tompkins, R. G. & Toner, M. Equilibrium separation and filtration of particles using differential inertial focusing. *Anal. Chem.* **80**, 2204-2211 (2008).